Penerbit Akademia Baru

Journal of Advanced Vehicle System

Journal homepage:
https://www.akademiabaru.com/submit/index.php/javs/index
ISSN: 2550-2212

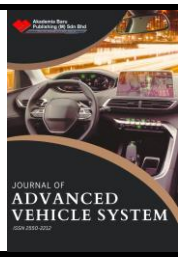

Battery Arrangement Analysis for Electric Vehicle using Air Cooling

Muhammad Faiq Irfan Mohd Farid[1], Fauziah Jerai[1,*], Nor Afifah Yahaya[1], Amalina Amir[1], Amir Radzi Ab Ghani[1], Hussain A. Alenezi[2]

[1] School of Mechanical Engineering, College of Engineering, Universiti Teknologi MARA, 4050 Shah Alam, Selangor, Malaysia
[2] Department of Manufacturing Engineering, College of Technological Studies, PAAET, 13092 Kuwait City, Kuwait

ABSTRACT

Effective thermal management is paramount for sustaining the optimal operational temperature of batteries in Electrical Vehicles (EV), thereby enhancing their longevity and ensuring both safety and performance. Air cooling, while being lightweight and economically feasible, frequently encounters difficulties in achieving adequate cooling efficacy, particularly under conditions of elevated load. Consequently, the optimization of battery pack design alongside air cooling configurations becomes imperative to tackle these challenges, thereby ensuring reliability, safety, and efficiency in electric vehicle applications. The objective of this research is to employ Computational Fluid Dynamics (CFD) analysis to ascertain the optimal arrangement of batteries for the enhancement of thermal performance and to pinpoint the ideal inlet location necessary to attain maximum thermal efficacy. The analysis evaluates square, staggered, and other innovative configurations to determine arrangements that optimize cooling efficiency and mitigate hotspots. The findings indicate that the battery configuration with a Staggered Arrangement produced the most favourable battery performance while maintaining uniformity in the temperature differential among cells within the arrangement. It is anticipated that the results of this investigation will facilitate the optimization of the battery thermal management system in electric vehicles, consequently enhancing battery lifespan and performance.

Keywords:
Computational Fluid Dynamics (CFD); CFD simulation for optimal battery inlet; battery arrangement optimization; air-cooled battery thermal management system

Received: 16 May 2024 **Revised: 20 July 2024** **Accepted: 28 August 2024** **Published: 30 September 2024**

1. Introduction

Batteries constitute a fundamental element in the operational efficacy and performance metrics of electric vehicles (EVs), acting as the principal energy storage mechanism that facilitates both propulsion and a variety of functional capabilities. Lithium-ion batteries are predominantly employed in EVs owing to their superior energy density, operational efficiency, and lightweight properties, which are critical for the enhancement of vehicle performance [1]. These batteries not only accumulate energy but also discharge it rapidly to accommodate fluctuating load requirements, thereby augmenting the overall efficiency and all-electric range of the vehicle [2]. Furthermore, a self-regulating battery model is essential for effective battery management strategies, guaranteeing optimal operational performance and safety by continuously monitoring battery conditions and

* *Corresponding author.*
E-mail address: fauziahjerail@uitm.edu.my

https://doi.org/10.37934/javs.15.2.116

mitigating risks such as overcharging or undercharging [3]. This holistic battery management system (BMS) bolsters the reliability and durability of the battery pack, which is imperative for the sustainable operation of EVs [4]. Consequently, the amalgamation of sophisticated battery technologies and management frameworks is crucial in enhancing electric vehicle functionalities and fostering environmental sustainability.

Thermal sensitivity exerts a substantial influence on the efficacy, safety, and durability of lithium-ion batteries. Fluctuations in ambient temperature can induce heterogeneous thermal gradients within the battery, thereby affecting electrochemical phenomena and potentially precipitating safety concerns such as thermal runaway [5]. Nevertheless, the thermal sensitivity inherent to these batteries detrimentally affects both their operational lifespan and overall efficacy [6]. Consequently, the optimal temperature range for battery operation is one that substantially augments both performance and durability [7]. The operational temperature range considered optimal for lithium-ion battery systems is restricted to 15°C to 35°C, with temperature variations not surpassing 5°C within a multi-cell module [8]. Conversely, temperature increases beyond 80°C may instigate irreversible reactions within the lithium-ion battery assembly, thereby exacerbating the risk of thermal runaway [9]. Thus, the creation of adequate temperature regulation systems for battery configurations is of utmost significance [10].

The battery's role in electric vehicles is critical, making the choice of a suitable battery essential for achieving optimal operational performance. Researchers have developed various methods to tackle thermal control challenges, such as air cooling, liquid cooling, PCMs, and heat pipe systems [11-13]. Furthermore, managing battery temperature has been found to improve the stability of charge and discharge cycles [14]. Pouch, cylindrical, and prismatic cells are common forms of lithium-ion batteries, while battery modules consist of cells connected in parallel or series [15-17]. Connecting cells in series results in a larger total battery voltage, while connecting them in parallel increases the overall battery capacity [18,19]. In addition, multiple research projects have been conducted to optimize the spacings between cylindrical or prismatic battery pack cells [20-22]. A study by Fan *et al.*, [23] revealed that a smaller gap spacing between cells in a prismatic cell battery causes a reduced temperature increase. In their findings, it was determined that a moderate gap spacing between the cells led to improved uniformity. Interestingly, even with uneven gap spacing, there was still an improvement in temperature distribution, although the reduction in temperature rise was minimal.

Recent advancements in thermal management systems for electric vehicle (EV) batteries have focused on optimizing battery performance based on their arrangement. The Battery Thermal Management System (BTMS) is crucial for regulating the temperature of lithium-ion batteries, which directly impacts their performance, safety, and lifespan [24]. Among the various BTMS technologies, the combined liquid system (CLS) and phase change material (PCM) cooling systems have emerged as effective solutions for managing battery thermal behavior [25]. The CLS utilizes liquid as a medium to efficiently dissipate heat from battery cells, ensuring optimal operating temperatures [25]. In contrast, the PCM cooling system leverages the thermal properties of phase change materials to stabilize battery temperatures during operation, which is particularly beneficial for maintaining performance under varying conditions [26]. Additionally, innovative systems like the evaporative battery cooling thermal management system (EC-BThMS) have been developed to maintain battery temperatures within the ideal range of 20°C to 40°C, thereby enhancing battery lifespan and performance [27]. This system addresses the critical need for effective thermal management in EVs, especially as temperature fluctuations can significantly affect battery efficiency and safety [24]. Overall, the integration of these advanced thermal management systems is pivotal in advancing EV

technology, ensuring that batteries operate efficiently and safely across diverse environmental conditions [26].

Optimizing the arrangement of batteries within an EV is critical for maximizing both its operational lifespan and overall performance. Despite advancements in optimizing battery arrangements for electric vehicles (EVs), there remains a significant gap in understanding how diverse battery configurations specifically impact the efficiency of air-cooling-based thermal management systems. Current studies largely focus on generic thermal performance but lack detailed analyses of cylindrical battery pack arrangements and their interplay with air inlet placement to achieve optimal cooling. Moreover, the literature inadequately addresses the integration of computational fluid dynamics (CFD) as a precise tool for identifying the most effective configurations to minimize temperature gradients and enhance cooling performance under realistic operating conditions. Addressing this gap could significantly advance EV battery pack design, improving both thermal efficiency and longevity. By employing CFD analysis, this study aims to determine the optimal battery arrangement and inlet location for achieving the highest possible thermal performance. This research aims to find the best way to arrange batteries in a cylindrical model battery pack, maximizing thermal performance by finding the optimal arrangement and identifying the best location for the inlet to achieve maximum thermal efficiency and optimal temperature.

2. Methodology

2.1 Pre-processing Stage

A 3D model showing the Battery Thermal Management System (BTMS) was created using Catia V5 software. The BTMS includes 24 cylindrical battery cells, a fluid zone, an inlet, and an outlet. The model featured the BTMS layout, encompassing the inlet, outlet, and battery cylinders. The size of the battery cylinder is 20 mm in circumference and 180 mm in height. 3 types of BTMS were drawn to analyze different battery arrangements, as shown in Figure 1, Figure 2 and Figure 3. In the meshing setup, the size of elements was set to 0.0028, producing 484803 number of elements and 389031 nodes. The boundary conditions were determined where the inlet boundary condition acted as the inlet for air flow to enter and dispersed throughout the battery pack while the outlet was set as an outlet boundary condition for air flow to escape from the battery pack.

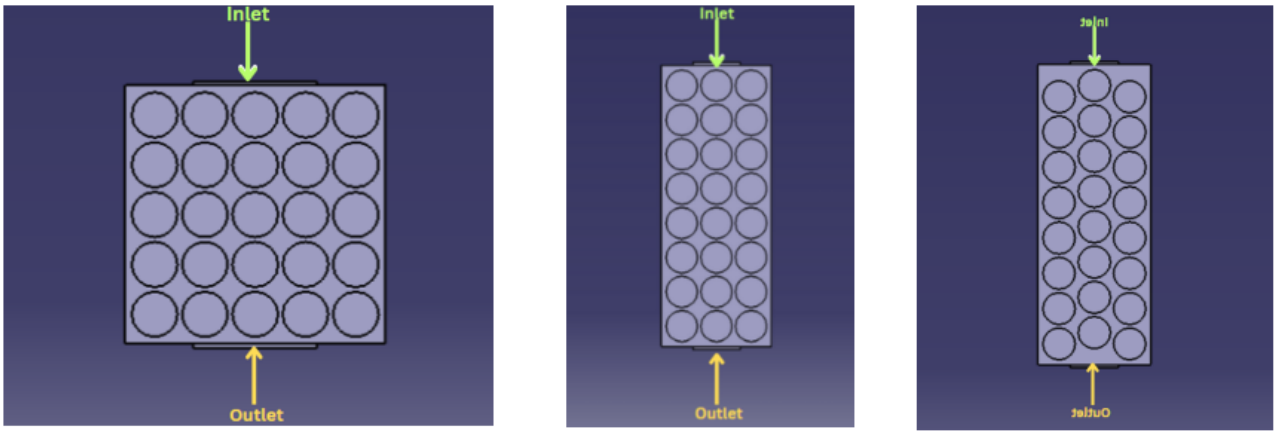

(a) (b) (c)

Fig. 1. Design 1 for (a) square, (b) 3x8 and (c) Staggered Arrangements

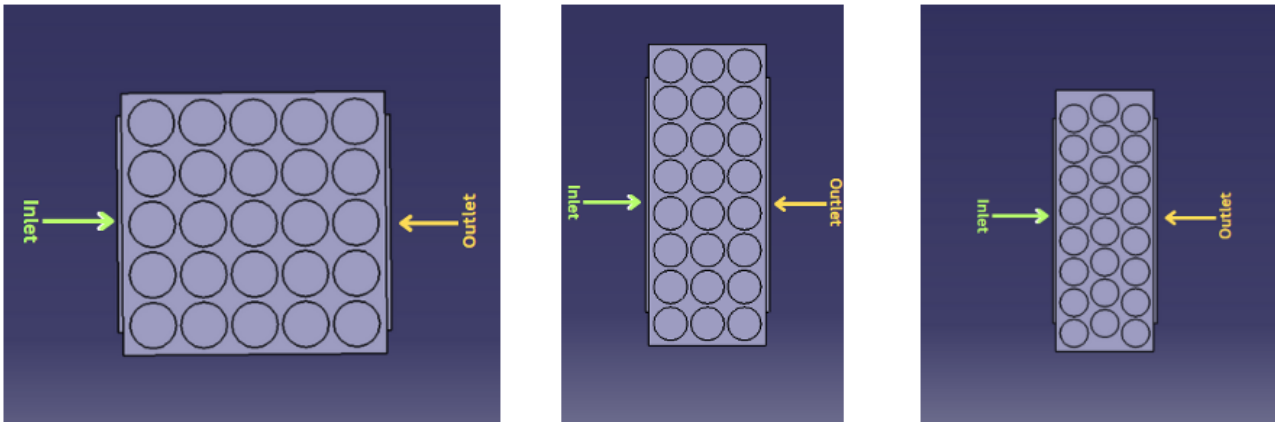

(a) (b) (c)

Fig. 2. Design 2 for (a) square, (b) 3x8 and (c) Staggered Arrangements

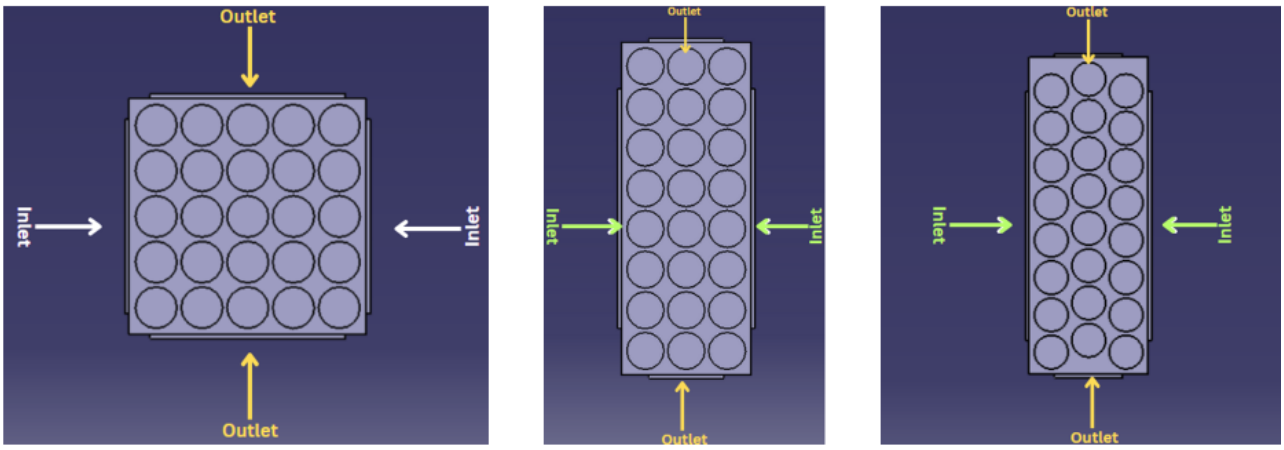

(a) (b) (c)

Fig. 3. Design 3 for (a) square, (b) 3x8 and (c) Staggered Arrangements

During the meshing stage, the type of boundary conditions is set as Figure 4 below, where the inlet is set as velocity-inlet, the cell boundary is set as wall and the outlet is set as pressure-outlet. The complete meshing can be observed in Figure 5 as shown below.

Fig. 4. Full size meshing of geometry and cylindrical cells

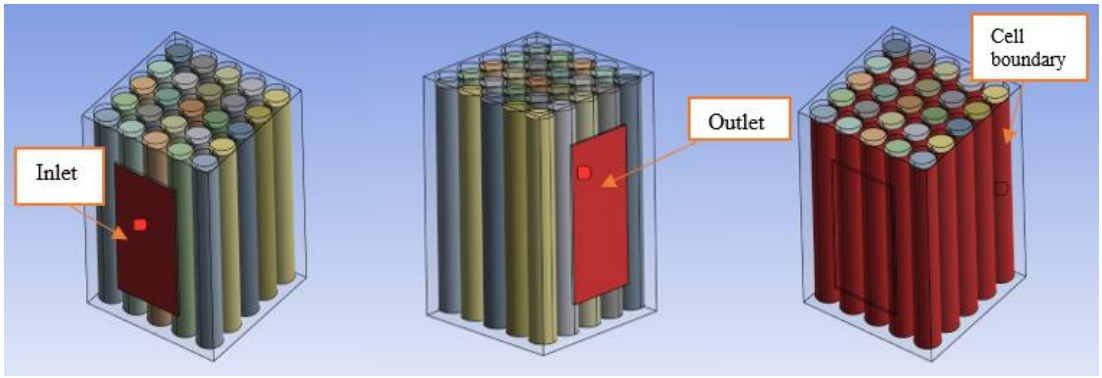

Fig. 5. Inlet, outlet and cell boundary named selection

2.2 Solver

All the inputs needed to perform the simulation were inserted where this is the setup stage before the calculation will be performed. Firstly, at this stage, a general setup is being done where the base of the solver will be chosen which in this case is the pressure-based solver. The gravitational acceleration is set at Z-Direction for a value of -9.81 m/s². The general setup for this case is shown in Table 1.

Table 1
General setup of the simulation

Solver	Parameter
Type	Pressure-based
Velocity formation	Absolute
Time	Transient
Gravitational acceleration	-9.81 m/s² at Z-direction

For this research, the K-epsilon turbulence model was chosen because of the shorter time for the solution to converge and the accuracy of it. Enhanced Wall Treatment for Near Wall Treatment was used for coarser mesh near walls to maintain accuracy [27]. Table 2 shows the summary of the viscous model for this simulation.

Table 2
Viscous Model

Model	Standard K-Epsilon
Near Wall Treatment	Enhanced Wall Treatment
Enhanced Wall Treatment options	Thermal effects
Options	Curvature correction

Solution initialization was done where there were initial conditions such as turbulence, pressure and velocity. In this case, the properties of lithium (as shown in Table 3) were defined where it includes the density and viscosity of the lithium as it is needed to simulate the movement. The least squared cell based is determined by the gradient in a cell, which minimizes the difference between the extrapolated values and the cell values when used to extrapolate the cell value to the centers of neighboring cells. As shown in Table 4, Second order upwind is chosen for momentum, turbulent kinetic energy, turbulent dissipation rate and energy because second-order are generally more accurate than first order. It is important to capture sharp gradients in the dissipation rate. First order

impact for transient formulation impact suitable for analyzing overall energy transfer and not detailed stress wave propagation.

Table 3
Lithium properties

Chemical formula	Li
Density [kg/m3]	900
Specific heat capacity, Co [J/kg K]	995
Thermal conductivity [W/m K]	5
Heat generation (W/m3)	5417

Table 4
Solution method

Scheme	SIMPLE
Flux Type	Rhie-Chow: Momentum based
Gradient	Least squares cell based
Pressure	Second order
Momentum	Second order upwind
Turbulent kinetic energy	Second order upwind
Turbulent dissipation rate energy	Second order upwind
Pseudo time method	Off
Transient formulation impact	First order impact

2.3 Governing Equations

Typically, the system's flow is turbulent. The following is an introduction to the Reynolds average Navier-Stokes equations using the k-turbulence model [28]:

$$\frac{\delta u_i}{\delta x_i} = 0 \tag{1}$$

$$\rho_a u_j \frac{\delta u_i}{\delta x_i} = \frac{\delta p}{\delta x_i} + \frac{\delta}{\delta x_j}\left[(\mu + \mu_t)\frac{\delta u_i}{\delta x_i}\right] \tag{2}$$

Realistic battery cells generate heat in response to changes in temperature, charge level, and discharge rate. Consequently, the temperature is determined using the transient temperature equations and the equations are shown below [28]:

$$\rho_a c_{p,a} \frac{\delta T_a}{\delta T} + \rho_a c_{p,a} u_j \frac{\delta T_a}{\delta x_j} = \frac{\delta}{\delta x_j}\left[\left(\lambda_2 + \frac{\mu_t}{\sigma_T}\right)\frac{\delta T_a}{\delta x_j}\right] \tag{3}$$

$$\rho_a c_{p,a} \frac{\delta T_b}{\delta t} = \frac{\delta}{\delta x_j}\left[\left(\lambda_{bj} + \frac{\delta T_b}{\delta x_j}\right)\right] + \Phi_b \tag{4}$$

where;

$$u_t = \rho C_u \frac{k^2}{\varepsilon} \tag{5}$$

$$C_u = 0.09, C_1 = 1.44, C_2 = 1.92, \sigma_k = 1.0, \sigma_\varepsilon = 1.3, \sigma_T = 0.85 \tag{6}$$

3. Results

3.1 Grid Independence Study

In grid independence study, the meshing of the BTMS geometry for all the designs which is the Type 1, Type 2 and Type 3 inlet locations where both velocities for the inlet are set at 1 m/s and the temperature at the inlet is 298 K were investigated (Table 5). The number of grids that will be used for the meshing and simulation was chosen from the grid independence study. This is a crucial step because the number of grids will determine both the overall computational cost and the accuracy of the result. In this case, the accuracy of the Navier-Stokes equation solution depends heavily on the quality of the grid, since the simulation's result is influenced by the solutions performed at each grid [13].

Table 5
Grid independence study

Inlet type	Discharge rate (W/m3)	Inlet velocity (m/s)	Inlet temperature (K)	Average battery temperature (K)	Number of elements
1	5417	1	298	305.79	216865
1	5417	1	298	304.48	416865
1	5417	1	298	303.99	616865
1	5417	1	298	303.99	854884
1	5417	1	298	303.99	1000379

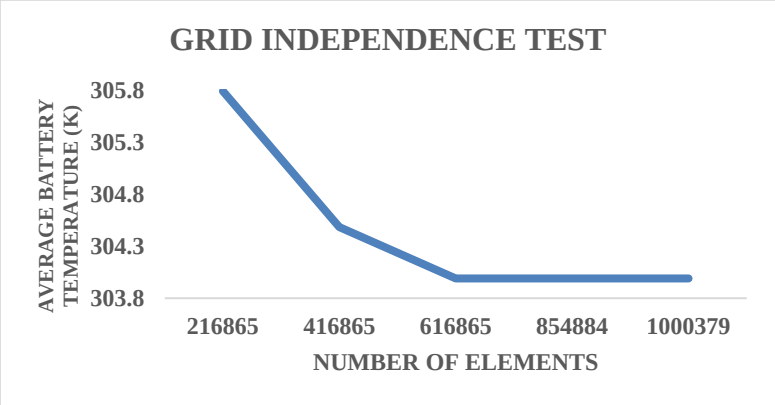

Fig. 6. Grid independence test

From the grid independence study, the number of grids chosen is 216865, 416865, 616865, 854884 and 1000379. Referring to Figure 6, the grid independence test shows that the number of elements 616865 starts to become constant. Hence, the number of elements chosen was 616865 for the simulation. By choosing the lower number of grids, the simulation can be completed faster than the higher number of grids, but with the higher number of grids, a more accurate average battery temperature can be obtained [29].

3.2 Cell Arrangement: 3x8 Arrangement

The effect of inlet velocity, discharge rate and inlet temperature on average battery temperature and maximum battery temperature for 3x8 Arrangement 1, 2 and 3 is shown in Table 6 below. In 3x8 Arrangement 1, the difference in average battery temperature for inlet temperatures 278 K and 288 K is 1.36 %. The difference in average battery temperature for inlet temperature 288 K and 298 K is 1.34%. The temperature values from the left side of the inlet increase towards the right side of the outlet. The temperature distribution is constant along the length of each cell. Figure 7(a), (b), and (c) below illustrate the effect of air inlet and outlet position on different planes using temperature contours. In 3x8 Arrangement 2, the difference in average battery temperature for inlet temperatures 278 K and 288 K is 0.14%. The difference in average battery temperature for inlet temperature 288 K and 298 K is 0.14%. The temperature values from the left side of the inlet increase towards the right side of the outlet. The temperature distribution is constant along the length of each cell. The effect of air inlet and outlet position on different plane is shown in Figure 7(d), (e) and (f), below using temperature contours. In 3x8 Arrangement 2, the difference in average battery temperature for inlet temperatures 278 K and 288 K is 0.15%. The difference in average battery temperature for inlet temperature 288 K and 298 K is 0.13%. The temperature values from left side of the inlet increase towards the right side of the outlet. The temperature distribution is constant along the length of each cell. Figures 7(g), (h), and (i) below illustrate the impact of air inlet and outlet placement on various plane, using temperature contours.

Table 6
3x8 arrangement type

Inlet Type	Discharge rate (W/m3)	Inlet velocity (m/s)	Inlet temperature (K)	Average battery temperature (K)	Max battery temperature (K)
1	5417	1	278	304.12	311.43
1	5417	1	288	308.31	314.00
1	5417	1	298	312.51	316.57
2	5417	1	278	320.96	321.97
2	5417	1	288	321.42	322.20
2	5417	1	298	321.87	322.43
3	5417	1	278	318.95	321.39
3	5417	1	288	319.86	321.69
3	5417	1	298	320.75	322.11

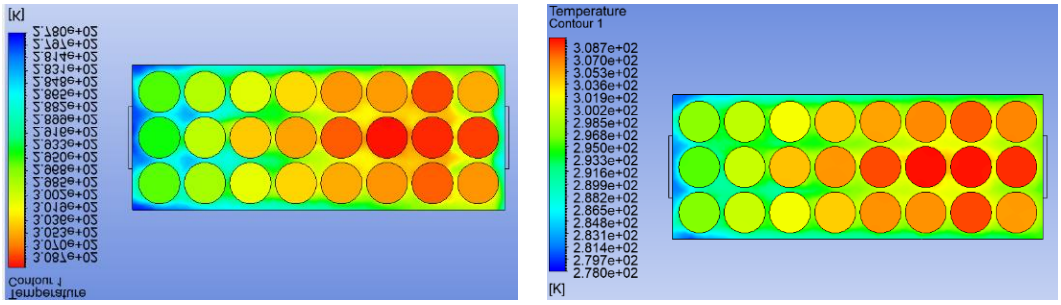

(a) (b)

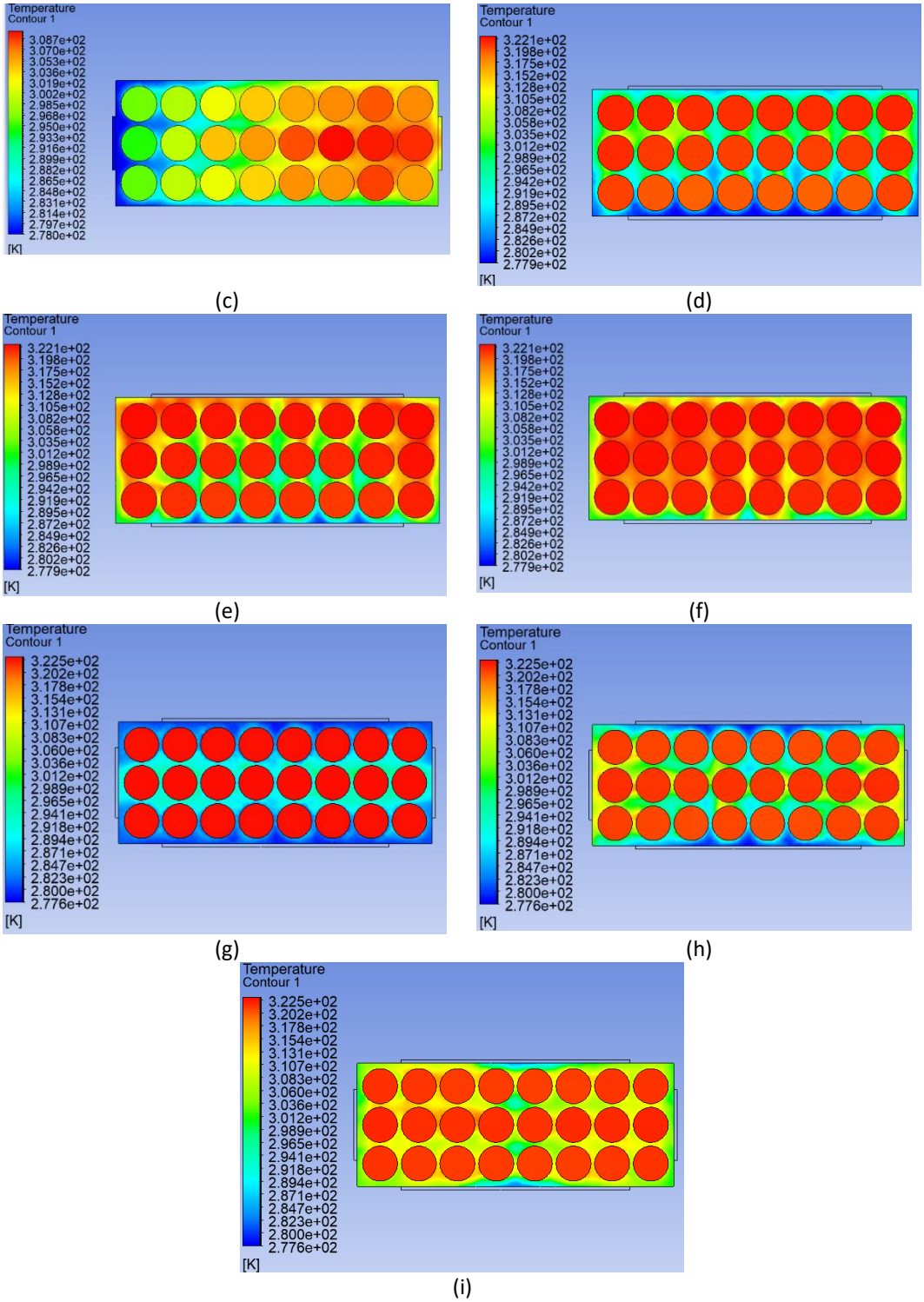

Fig. 7. Temperature contour in 3x8 Arrangement, (a) Type 1 at Plane XY, Z=5mm , (b) Type 1 at Plane XY, Z = 100mm, (c) Type 1 at Plane XY, Z=150mm, (d) Type 2 at Plane XY, Z=5mm (e) Type 2 at Plane XY, Z = 100mm, (f) Type 2 at Plane XY, Z=150mm, (g) Type 3 at Plane XY, Z=5mm (h) Type 3 at Plane XY, Z = 100mm, (i) Type 3 at Plane XY, Z=150mm

3.2 Cell Arrangement: Square Arrangement

The influence of inlet velocity, discharge rate, and inlet temperature on the mean battery temperature as well as the peak battery temperature for the Square Arrangement is delineated in Table 7 presented below. In the context of Square Arrangement 1, the variation in mean battery temperature between inlet temperatures of 278 K and 288 K is calculated to be 1.55%. Furthermore, the difference in mean battery temperature between inlet temperatures of 288 K and 298 K is determined to be 1.52%. The thermal values observed on the left side of the inlet exhibit an increase towards the right side of the outlet. The thermal distribution remains uniform along the longitudinal axis of each cell. The ramifications of the positioning of air inlets and outlets on various planes are illustrated in Figure 8(a), (b), and (c) below, utilizing temperature contours. In Square Arrangement 2, the variation in mean battery temperature for inlet temperatures of 278 K and 288 K is found to be 0.14%.

Table 7
Square arrangement type

Inlet type	Discharge rate (W/m3)	Inlet velocity (m/s)	Inlet temperature (K)	Average battery temperature (K)	Max battery temperature (K)
1	5417	1	278	306.52	312.77
1	5417	1	288	311.34	315.51
1	5417	1	298	316.16	319.41
2	5417	1	278	320.96	312.97
2	5417	1	288	321.42	322.20
2	5417	1	298	321.87	322.43
3	5417	1	278	318.95	321.39
3	5417	1	288	319.86	321.69
3	5417	1	298	320.75	322.11

Additionally, the difference in mean battery temperature for inlet temperatures of 288 K and 298 K is also 0.14%. The thermal values on the left side of the inlet again rise towards the right side of the outlet. The temperature distribution maintains its constancy along the length of each cell. The implications of air inlet and outlet positioning on distinct planes are depicted in Figure 8(d), (e), and (f) below, employing temperature contours. In Square Arrangement 3, the difference in mean battery temperature between inlet temperatures of 278 K and 288 K is noted to be 0.28%. Similarly, the difference in mean battery temperature for inlet temperatures of 288 K and 298 K stands at 0.28%. The thermal values from the left side of the inlet consistently increase towards the right side of the outlet. The temperature distribution is uniform along the length of each cell. The influence of the positioning of air inlets and outlets on various planes is depicted in Figure 8(g), (h), and (i) below, utilizing temperature contours.

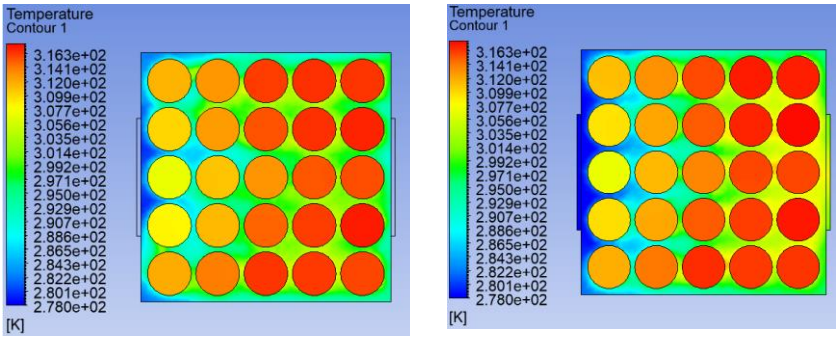

(a) (b)

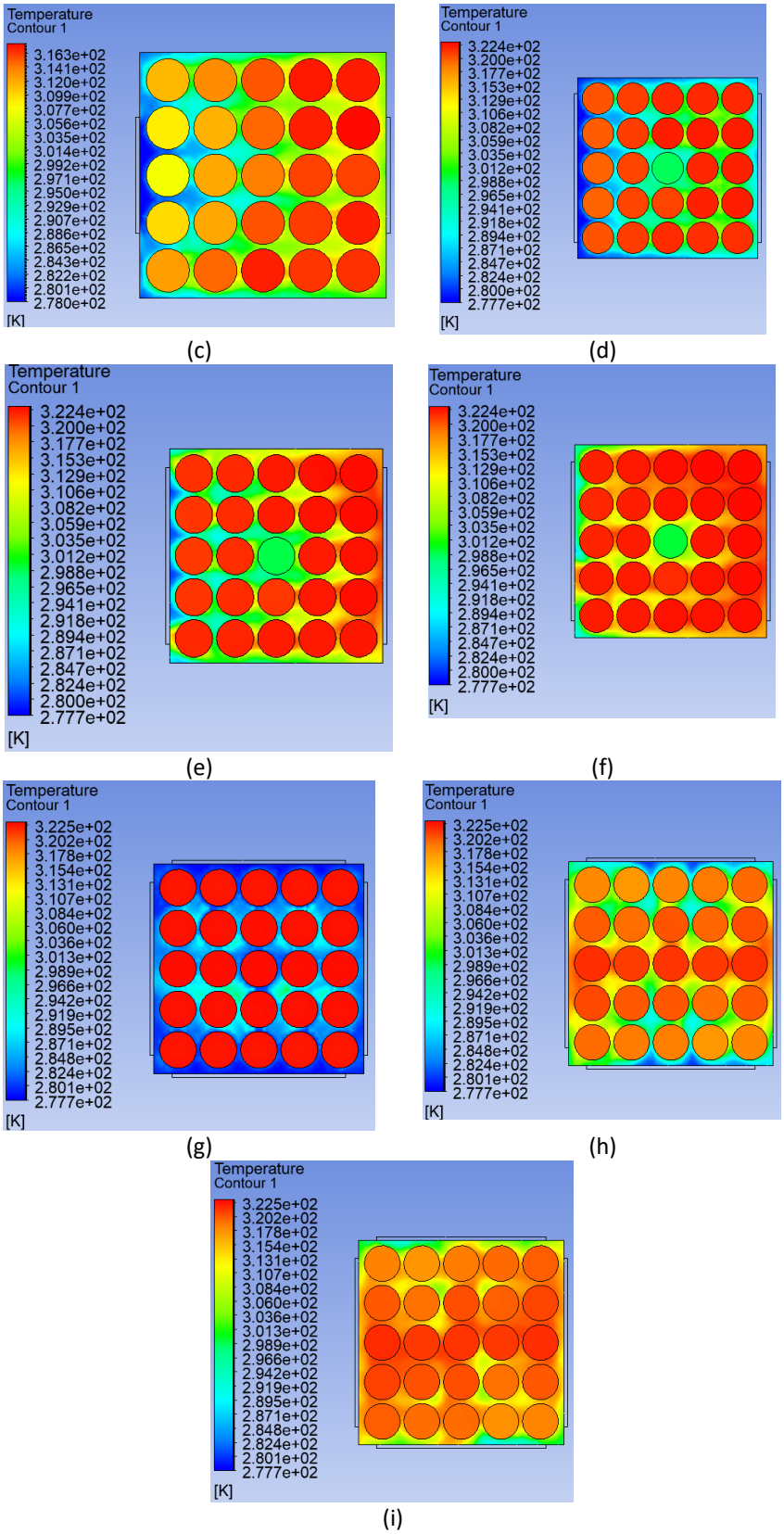

Fig. 8. Temperature contour in Square Arrangement, (a) Type 1 at Plane XY, Z=5mm , (b) Type 1 at Plane XY, Z = 100mm, (c) Type 1 at Plane XY, Z=150mm, (d) Type 2 at Plane XY, Z=5mm (e) Type 2 at Plane XY, Z = 100mm, (f) Type 2 at Plane XY, Z=150mm, (g) Type 3 at Plane XY, Z=5mm (h) Type 3 at Plane XY, Z = 100mm, (i) Type 3 at Plane XY, Z=150mm

3.2 Cell Arrangement: Staggered Arrangement

Table 8
Staggered Arrangement type

Inlet type	Discharge rate (W/m3)	Inlet velocity (m/s)	Inlet temperature (K)	Average battery temperature (K)	Max battery temperature (K)
1	5417	1	278	304.00	310.85
1	5417	1	288	308.22	313.55
1	5417	1	298	312.44	315.56
2	5417	1	278	314.61	321.77
2	5417	1	288	316.48	321.77
2	5417	1	298	318.34	322.21
3	5417	1	278	320.80	321.42
3	5417	1	288	321.29	321.76
3	5417	1	298	321.78	322.12

The influence of inlet velocity, discharge rate, and inlet temperature on both the average battery temperature and the maximum battery temperature for the Staggered Arrangement is delineated in Table 8 presented above. In Staggered Arrangement 1, the variation in average battery temperature between inlet temperatures of 278 K and 288 K amounts to 1.34%. Similarly, the variation in average battery temperature between inlet temperatures of 288 K and 298 K is also recorded as 1.34%. The temperature values exhibit an increasing trend from the left side of the inlet toward the right side of the outlet. Furthermore, the temperature distribution remains uniform along the entire length of each cell. The impact of the positioning of air inlets and outlets across different planes is illustrated in Figure 9(a), (b), and (c) below, utilizing temperature contours.

In Staggered Arrangement 2, the difference in average battery temperature between inlet temperatures of 278 K and 288 K is quantified as 1.36%. The discrepancy in average battery temperature between inlet temperatures of 288 K and 298 K is recorded as 1.34%. The temperature values manifest an increasing trend from the left side of the inlet to the right side of the outlet. The temperature distribution remains consistent throughout the length of each cell. The influence of the spatial arrangement of air inlets and outlets across varying planes is depicted in Figure 9(d), (e), and (f) below, employing temperature contours. In Staggered Arrangement 3, a measurement was conducted to determine the difference in average battery temperature between inlet temperatures of 278 K and 288 K, which resulted in a measurement of 0.15%. Additionally, another observation was made for the difference in average battery temperature between inlet temperatures of 288 K and 298 K, also measuring at 0.15%. The temperature values from the left side of the inlet progressively increase towards the right side of the outlet. Additionally, the temperature distribution is maintained uniformly along the length of each cell. The effect of the configuration of air inlets and outlets on different planes is represented in Figure 9(g), (h), and (i) below through the use of temperature contours.

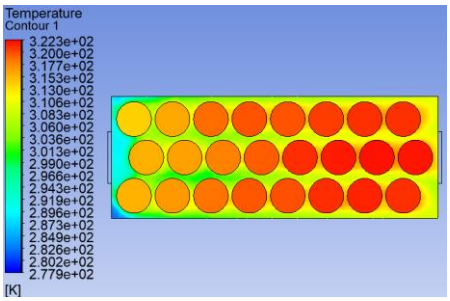

(a)

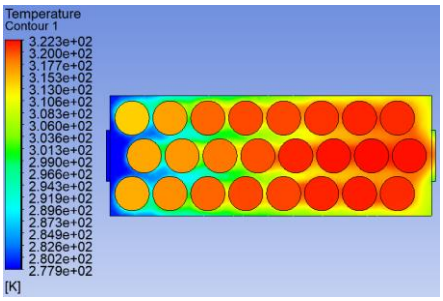

(b)

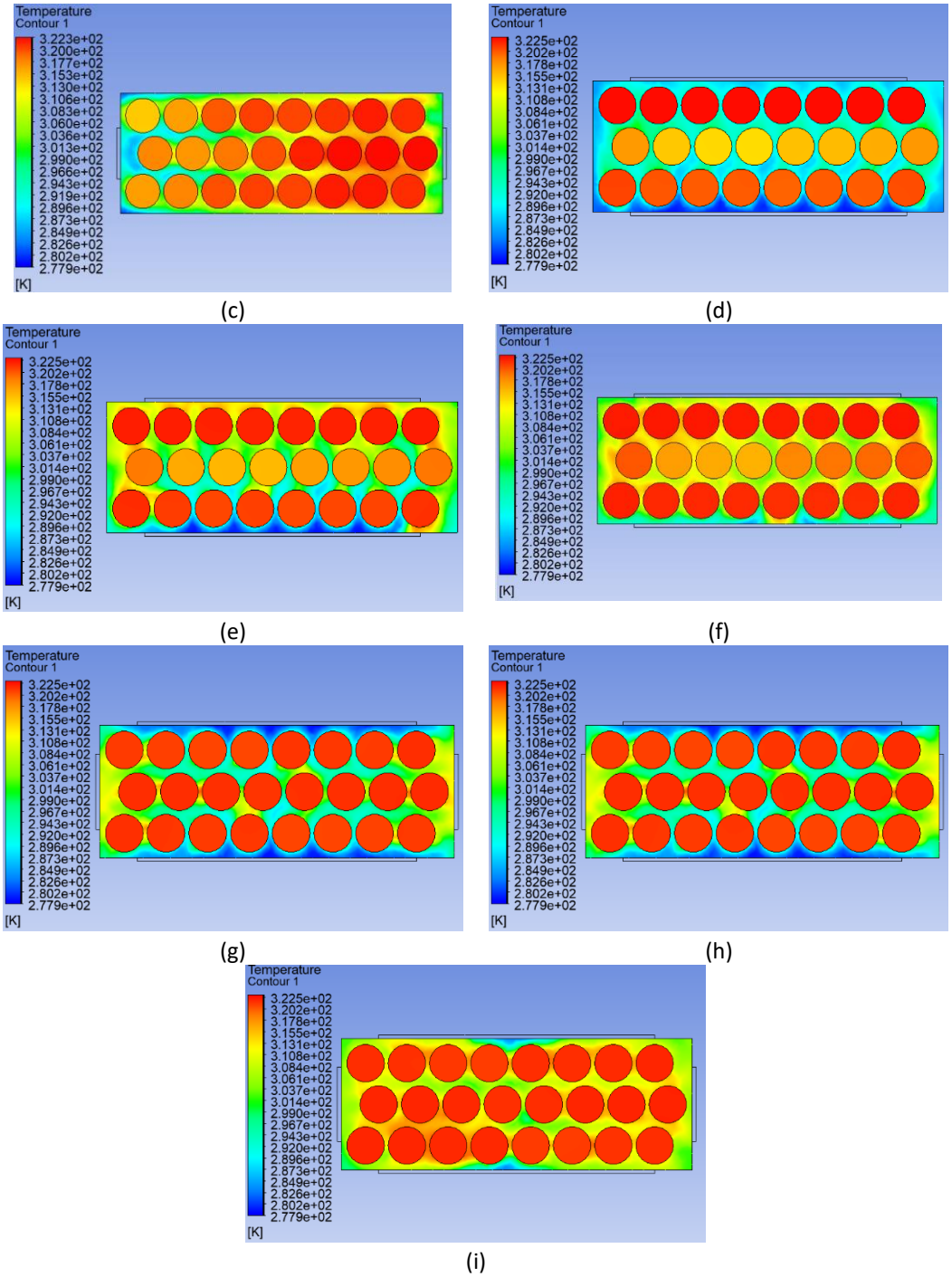

Fig. 9. Temperature contour in Staggered Arrangement, (a) Type 1 at Plane XY, Z=5mm , (b) Type 1 at Plane XY, Z = 100mm, (c) Type 1 at Plane XY, Z=150mm, (d) Type 2 at Plane XY, Z=5mm (e) Type 2 at Plane XY, Z = 100mm, (f) Type 2 at Plane XY, Z=150mm, (g) Type 3 at Plane XY, Z=5mm (h) Type 3 at Plane XY, Z = 100mm, (i) Type 3 at Plane XY, Z=150mm

3.1 Average Battery Temperature

Figure 10 shows the average battery temperature for every battery arrangement in different Inlet types. It can be observed that Inlet Position 1 has the lowest average battery temperature in comparison to Position 2 and Position 3. Similarly, the Staggered Arrangement exhibits the lowest average battery temperature when compared to the Square and 3x8 Arrangement. In Staggered

Arrangement, it is evident that Type 1 has the lowest average battery temperature compared to Type 2 and Type 3.

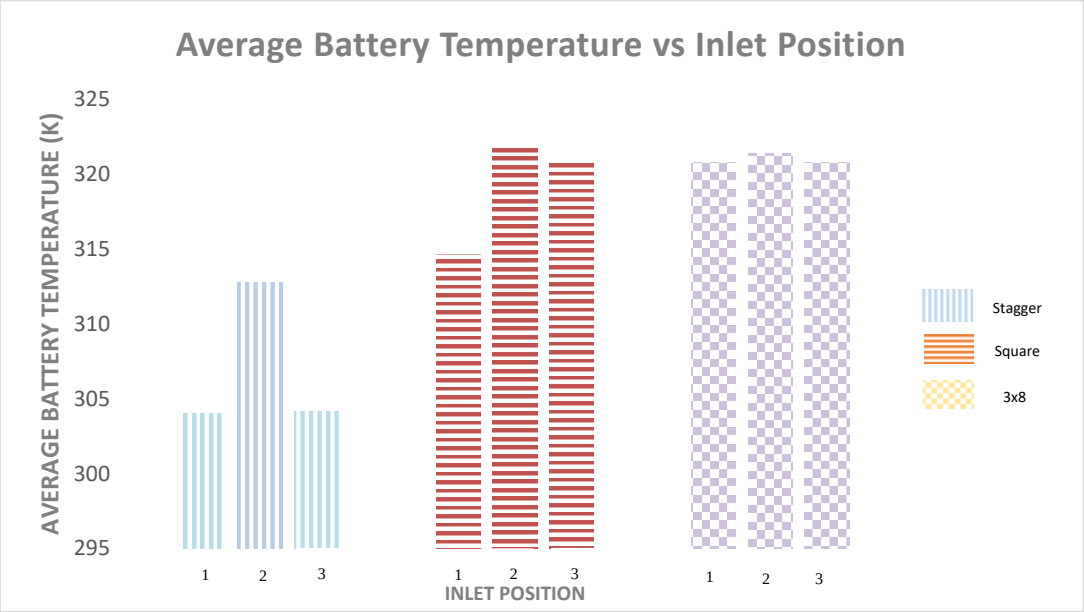

Fig. 10. Average battery temperature for every battery arrangement in different inlet types

The results obtained from the present analytical study on battery cylinder configurations yield significant implications for the optimization of the design and operational efficacy of electric vehicles (EVs). The investigation has effectively demonstrated that Staggered Arrangement Type 1 within the staggered configurations achieves the most uniform thermal distribution among the cells. This is crucial for ensuring balanced discharge rates and averting localized overheating or cold spots. Additionally, these arrangements can be customized for varying discharge rates and airflow velocities, allowing them to accommodate a wide range of operational conditions. The findings highlight the potential of air-cooling systems in EVs, offering a simpler and less expensive alternative to liquid-cooling while achieving comparable efficiency. Moreover, the insights derived can also facilitate the advancement of modular battery architectures for future EVs, optimizing manufacturing processes and enabling scalability across diverse vehicle categories. These refined designs not only bolster energy efficiency and reliability but also contribute to the comprehensive sustainability of electric vehicle technology and potential alliances between higher education and industry.

4. Conclusions

This study has successfully conducted the simulation to investigate the CFD analysis in battery arrangement in EV using air cooling. The study focuses on the average battery temperature of the battery after cooling.

CFD analysis of the battery cylinder in an electric vehicle has been conducted to analyse and optimize the design of the battery thermal management system. A battery module containing 24 cells is arranged in 3x8, square and Staggered Arrangement. The effect of each arrangement on the average and maximum temperature of the battery module at different velocity and discharge rates are observed. It is crucial to maintain a consistent temperature both inside the battery module and along the length of cells, in addition to keep the temperature within the allowed range. Based on the study, the average temperature of the battery is the lowest for Staggered Arrangement compared to

Square and 3x8 Arrangement. In Staggered Arrangement, it is evident that Type 1 has the lowest average battery temperature compared to Type 2 and Type 3.

Acknowledgement
This research was not funded by any grant

References
[1] Yang, Shichun, Xinhua Liu, Shen Li, and Cheng Zhang. "Vehicle Applications." In *Advanced Battery Management System for Electric Vehicles*, pp. 271-279. Singapore: Springer Nature Singapore, 2022. https://doi.org/10.1007/978-981-19-3490-2_14

[2] Júnior, Carlos Antônio Rufino, Eleonora Riva Sanseverino, Pierluigi Gallo, Murilo Machado Amaral, Daniel Koch, Yash Kotak, Sergej Diel, Walter Gero, Hans-Georg Schweiger, and Hudson Zanin. "A Comprehensive Review of EV Lithium-Ion Battery Degradation." (2023).

[3] Dhote, Aparna B, "Selection of Li-Ion Batteries Used On Electric Vehicles." *Building Materials and Engineering Structures* 2, no. 2 (2024): 01-06. https://doi.org/10.46632/bmes/2/2/1

[4] Abutalaha, Inamdar., Vipashana, Kharate., Abhishekkumar, Singh., Ashwini, Farad. "Electric Vehicle Battery Management System with Charge Monitor and Fire Protection." *International Journal of Advanced Research in Science, Communication and Technology*. 3 (2024). https://doi.org/10.48175/IJARSCT-18339

[5] Bamrah, Parush, Manish Kumar Chauhan, and Basant Singh Sikarwar. "CFD analysis of battery thermal management system." In *Journal of Physics: Conference Series*, vol. 2178, no. 1, p. 012035. IOP Publishing, 2022. https://doi.org/10.1088/1742-6596/2178/1/012035

[6] Ishtiaque, MD Mahdi UL, Jayanth R. Ramamurthy, Cary L. Pint, and Todd A. Kingston. "Quantifying the Thermo-Electrochemical Sensitivity of Li-Ion Batteries to Modulating Interelectrode Thermal Gradients." In *Electrochemical Society Meeting Abstracts 242*, no. 3, pp. 348-348. The Electrochemical Society, Inc., 2022. https://doi.org/10.1149/MA2022-023348mtgabs

[7] Wang, Junjie, Wenxin Mei, Binbin Mao, and Qingsong Wang. "Investigation on the temperature control performance and optimization strategy of a battery thermal management system combining phase change and liquid cooling." *Applied Thermal Engineering* 232 (2023): 121080. https://doi.org/10.1016/j.applthermaleng.2023.121080

[8] Kumar, Suresh, OM Prakash Shukla, and Jaydeep Shah. "Thermal management lithium-ion battery for electric vehicles with using cold plate." *World Journal of Advanced Engineering Technology and Sciences* 12, no. 1 (2024): 087-094. https://doi.org/10.30574/wjaets.2024.12.1.0191

[9] Sun, Zeyu, Yue Guo, Cheng Zhang, Hongming Xu, Quan Zhou, and Chongming Wang. "A novel hybrid battery thermal management system for prevention of thermal runaway propagation." *IEEE Transactions on Transportation Electrification* 9, no. 4 (2022): 5028-5038. https://doi.org/10.1109/TTE.2022.3215691

[10] Wang, Qian, Bin Jiang, Bo Li, and Yuying Yan. "A critical review of thermal management models and solutions of lithium-ion batteries for the development of pure electric vehicles." *Renewable and Sustainable Energy Reviews* 64 (2016): 106-128. https://doi.org/10.1016/j.rser.2016.05.033

[11] Zuber, Mohammad, K. N. Chethan, Laxmikant G. Keni, Irfan Anjum Badruddin Magami, and Chandrakant R. Kini. "Enhancing Electric Vehicle Battery Thermal Management using Phase Change Materials: A CFD Analysis for Improved Heat Dissipation." *CFD Letters* 16, no. 8 (2024): 138-149. https://doi.org/10.37934/cfdl.16.8.138149

[12] Nasir, Faiza Mohamed, Mohd Zulkifly Abdullah, and Mohd Azmi Ismail. "Effect of heat pipe's configuration in managing the temperature of EV battery." *CFD Letters* 15, no. 3 (2023): 22-34. https://doi.org/10.37934/cfdl.15.3.2234

[13] Soliman, Mohamed Hassan. "Performance of a Novel Thermal Management System of Li-Ion Batteries Used in Electric Vehicles." *Assiut University Bulletin for Environmental Researches* 27, no. 1 (2024): 100-112.

[14] Razi, Muhammad Fikri Irsyad Mat, Zul Hilmi Che Daud, Zainab Asus, Izhari Izmi Mazali, Anuar Abu Bakar, and Mohd Kameil Abdul Hamid. "Li-NMC Temperature Modelling Based on Realistic Internal Resistance." *CFD Letters* 16, no. 12 (2024): 140-148. https://doi.org/10.37934/cfdl.16.12.140148

[15] Venkatesh, R. J., Vara Prasad Bhemuni, Dilip Shyam Prakash Chinnam, and M. D. Mohan Gift. "Optimizing Hybrid Active–Passive Thermal Management of Prismatic Li-Ion Batteries Using Phase Change Materials and Porous-Filled Mini-Channels." *Energy Storage* 6, no. 7 (2024): e70060. https://doi.org/10.1002/est2.70060

[16] Zhang, Yansen, Weikuo Zhang, and Wenjun Kong. "Numerical and experimental study on thermal behavior of prismatic lithium-ion battery for large-capacity energy storage." *Journal of Energy Storage* 83 (2024): 110620. https://doi.org/10.1016/j.est.2024.110620

[17] Liu, Yang, Jian-Ming Li, Qing Ma, and Ya-Xiong Wang. "Simulation and analysis of a noval thermal management system integrated with heat pipe radiators for 4680 battery module." *Thermal Science* 00 (2024): 137-137. https://doi.org/10.2298/TSCI240201137L

[18] Wang, Yongqi, Yujie Zhao, Siyuan Zhou, Qingzhong Yan, Han Zhan, Yong Cheng, and Wei Yin. "Impact of individual cell parameter difference on the performance of series–parallel battery packs." *ACS omega* 8, no. 11 (2023): 10512-10524. https://doi.org/10.1021/acsomega.3c00266

[19] Luan, Chunxiao, Chen Ma, Chunyu Wang, Long Chang, Linjing Xiao, Zhihao Yu, and Hongyu Li. "Influence of the connection topology on the performance of lithium-ion battery pack under cell-to-cell parameters variations." *Journal of Energy Storage* 41 (2021): 102896. https://doi.org/10.1016/j.est.2021.102896

[20] Li, Haibing, Yaoliang Ye, Zhenjie Zhang, Wei Yu, Zhongbo Zhang, and Wenbo Zhu. "Investigating the impact of battery arrangements on thermal management performance of lithium-ion battery pack design." *Advances in Mechanical Engineering* 16, no. 9 (2024): 16878132241272144. https://doi.org/10.1177/16878132241272144

[21] Ghafoor, Usman, Muhammad Waqas Yaqub, Muhammad Uzair Qureshi, and Muhammad Nouman Aslam Khan. "Thermal optimization of Li-ion battery pack using genetic algorithm integrated with machine learning." *Thermal Science and Engineering Progress* 44 (2023): 102069. https://doi.org/10.1016/j.tsep.2023.102069

[22] Liu, Zheng, Jiaxin Wu, Wuchen Fu, Pouya Kabirzadeh, Sara Kohtz, Nenad Miljkovic, Yumeng Li, and Pingfeng Wang. "Generative design and optimization of battery packs with active immersion cooling." In *2023 IEEE Transportation Electrification Conference & Expo (ITEC)*, pp. 1-5. IEEE, 2023. https://doi.org/10.1109/ITEC55900.2023.10187078

[23] Chen, Kai, Zhenli Zhang, Bingheng Wu, Mengxuan Song, and Xiaoling Wu. "An air-cooled system with a control strategy for efficient battery thermal management." *Applied Thermal Engineering* 236 (2024): 121578. https://doi.org/10.1016/j.applthermaleng.2023.121578

[24] Liu, Meng, Xulong Li, Runda Qian, Xitao Lu, Yifan Liu, and Deqiu Zou. "All-Climate Thermal Management Performance of Power Batteries Based on Double-Layer Flexible Phase Change Materials." *Advanced Functional Materials* (2024): 2415370. https://doi.org/10.1002/adfm.202415370

[25] Tai, Le Duc, Kunal Sandip Garud, Seong-Guk Hwang, and Moo-Yeon Lee. "A Review on Advanced Battery Thermal Management Systems for Fast Charging in Electric Vehicles." *Batteries* 10, no. 10 (2024): 372. https://doi.org/10.3390/batteries10100372

[26] Seyfi, Sevinc., Toygun, Dağdevir. "Research Progress of Battery Thermal Management Systems with Minichannels." *Energy, Environment and Storage* 3 (2024):109-115. https://doi.org/10.52924/EUYV2071

[27] Nazif, Hamid Reza, Hassan Basirat Tabrizi, and Farhad A. Farhadpour. "Comparative analysis of the boundary transfer method with other near-wall treatments based on the k–ε turbulence model." *European Journal of Mechanics-B/Fluids* 44 (2014): 22-31. https://doi.org/10.1016/j.euromechflu.2013.10.001

[28] Chen, Kai, Yiming Chen, Yiqi She, Mengxuan Song, Shuangfeng Wang, and Lin Chen. "Construction of effective symmetrical air-cooled system for battery thermal management." *Applied Thermal Engineering* 166 (2020): 114679. https://doi.org/10.1016/j.applthermaleng.2019.114679

[29] Lee, Minhyung, Gwanyong Park, Changyoung Park, and Changmin Kim. "Improvement of grid independence test for computational fluid dynamics model of building based on grid resolution." *Advances in Civil Engineering* 2020, no. 1 (2020): 8827936. https://doi.org/10.1155/2020/8827936